Sensors and Actuators Reports 10 (2025) 100375

Contents lists available at ScienceDirect

Sensors and Actuators Reports

journal homepage: www.sciencedirect.com/journal/sensors-and-actuators-reports

Molecularly imprinted poly(o-aminophenol)-based electrochemical sensor for the quantitative detection of a VP28 biomarker for white spot syndrome virus

Young-Ran Yun [a], Hyoung Jun Kim [b], Sung Yang [a,*]

[a] School of Mechanical and Robotics Engineering, Gwangju Institute of Science and Technology (GIST), Gwangju 61005, Republic of Korea
[b] WOAH Reference Laboratory for VHS, National Institute of Fisheries Science, Busan 46083, Republic of Korea

ARTICLE INFO

Keywords:
White Spot Syndrome Virus (WSSV)
VP28 biomarker
Molecularly Imprinted Polymer (MIP)
Electrochemical sensor
Poly(o-aminophenol)

ABSTRACT

White spot syndrome virus (WSSV) is a deadly pathogen that can cause mass mortality within several days. VP28, known as a biomarker of WSSV, accounts for over half of the total envelope protein. It plays a crucial role in viral infection and is a useful diagnostic indicator for immunological detection.

Here, we developed a molecularly imprinted polymer (MIP)-based electrochemical sensor using a gold nanostructured electrode and assessed its performance in detecting VP28. The electropolymerized poly(o-aminophenol) film supplies specific binding sites complementary to VP28. The molecularly imprinted cavities were examined using electrochemical analysis to confirm their ability to recognize the target molecule. The sensor generates a response signal through label-free sensing with a redox probe. It demonstrated a detection limit of 7.01 ng/mL (S/N = 3) and an imprinting factor of 4.25 at 0.78–50 ng/mL concentrations. The selectivity study revealed a response signal 4.5 times higher for the target molecule than for interfering substances. Compared with the standard PCR method for real samples, the MIP-based sensor performed similarly according to virus concentration. These findings suggested that the MIP-based sensor is a simple and suitable alternative to conventional WSSV detection methods. This electrochemical sensing platform with electropolymerization of the molecularly imprinted polymer can promote the detection and monitoring of WSSV expressing VP28.

1. Introduction

White spot syndrome virus (WSSV) can cause substantial economic losses in shrimp farming and kill up to 100 % of infected individuals within 10 days [1,2]. Without a reliable vaccine, the most efficient method for preventing infection is rapidly isolating infected individuals [3]. Polymer chain reaction (PCR) is a conventional method limited by the need for complex equipment, long assay times, and expensive materials. Therefore, further research is needed to develop an effective diagnostic platform for the rapid, sensitive, simple, and accurate detection of WSSV.

Molecularly imprinted polymer (MIP)-based electrochemical sensors have recently gained attention in biomarker detection research [4–6]. This sensor uses synthetic recognition elements to detect target disease markers. It does not require specific biorecognition elements and complex biomanufacturing processes, whereas ELISA and LFA rely on antibodies or ligands. MIP-based sensors are especially promising for use in point-of-care testing and resource-limited environments, given their short turnaround time, low sample requirements, relatively high sensitivity and selectivity, and cost-effectiveness [7]. Its application can be expanded to various macromolecules, such as proteins and bacteria [8–11]; however, the fabrication of MIP-based sensors for macromolecule detection has several challenges, including physicochemical complexity, morphological instability, difficulties in template removal, lack of appropriate functional monomers, and particular polymerization conditions [12–14].

This study used ortho-aminophenol (o-AP) as a functional monomer because it displays several advantages over other electroactive

Abbreviations: IF, Imprinting factor; MIP, Molecularly imprinted polymer; NIP, Non-molecularly imprinted polymer; P(o-AP), Polymerized o-aminophenol; WSSV, White spot syndrome virus.

* Corresponding author at: School of Mechanical and Robotics Engineering, Gwangju Institute of Science and Technology (GIST), Gwangju 61005, Republic of Korea.
E-mail address: syang@gist.ac.kr (S. Yang).

https://doi.org/10.1016/j.snr.2025.100375
Received 10 June 2025; Received in revised form 7 August 2025; Accepted 16 August 2025
Available online 17 August 2025

polymers. o-AP can be synthesized through its hydroxyl or amine groups at the pH medium and controlled within a nanoscale thickness owing to its self-limiting growth. Based on the similar electropolymerization conditions reported in a previous study [15], the thickness of the electropolymerized o-AP is estimated to range from approximately 5 to 35 nm.

For these reasons, other studies have reported the electropolymerized MIP sensor using the o-AP as an artificial recognition element [16–19].

VP28 is one of the major envelope proteins (MW = 28 kDa) with a calculated isoelectric point of 4.7. This is critical in viral infection and is widely studied for developing vaccines and molecular-based diagnostics [20–22]. In this study, VP28 was used as a template molecule for molecular imprinting. Similarly, previous studies have reported that MIP sensors are designed to recognize specific protein-based biomarkers rather than whole viruses [23–26].

MIP synthesis was optimized and validated based on the relevant electrochemical characteristics. The template immobilization process and electropolymerization conditions are crucial for fabricating the MIP-based sensor.

There are two methods for immobilizing template molecules on an electrode: Physical adsorption is a straightforward procedure, but it can cause the random arrangement of template molecules on the electrode surface, leading to non-uniform recognition sites and non-specific binding [27,28]. In contrast, chemical bonding can align the template molecules using a self-assembled monolayer (SAM), improving recognition site uniformity [29]. Therefore, we applied chemical bonding using a SAM to promote stable template immobilization and selectivity.

Polymer synthesis involves covalent bonding, non-covalent interactions, ion exchange, and electropolymerization. Electropolymerization is widely applied in electrochemical biosensors due to its compatibility and controllability with electrochemical systems [30,31]. This approach can directly synthesize polymer films onto the electrode surface with precise thickness and density via an external current. MIP-based sensors fabricated using electropolymerization have shown good sensitivity and selectivity [32]. Accordingly, we utilized electropolymerization for MIP film synthesis.

We selected gold nanostructured electrodes for their large surface area and high conductivity to enhance electrochemical activity. It promotes active interactions between the electrode surface and polymer matrix, improving the response signal [33–35]. Moreover, the modified electrode facilitates the removal of template molecules within the polymer matrix, increasing sensitivity and reproducibility [36].

This study presents a molecularly imprinted poly *o*-aminophenol (o-AP)-based electrochemical sensor for detecting VP28 as a biomarker of WSSV. This research aims to provide a practical sensor for virus detection in time-constrained and/or resource-limited settings. Under strictly controlled conditions, the MIP-based electrochemical sensor showed a low limit of detection (LoD) and good selectivity for VP28, which was confirmed through electrochemical signal responses. We validated the MIP-based sensor using real samples and found that it offered good sensitivity and selectivity with a fast and straightforward assay process that enables real-time detection. This sensor is expected to be useful in detecting various infectious diseases in industrial and clinical contexts.

2. Materials and methods

2.1. Chemicals and materials

Electrochemical signal measurements were performed using a CHI760D electrochemical workstation (CH Instruments, Austin, TX, USA). The three-electrode system consisted of a platinum wire counter, an Ag/AgCl reference, and a gold-nanostructured working electrode chip. The working electrode chip was fabricated using conventional microfabrication. The patterned plain gold electrode of 2 mm diameter was modified by an electroless plating method following the previously reported [37].

The reagents included 3-mercaptopropionic acid (3-MPA), 1-ethyl-3-(3-dimethylaminopropyl) carbodiimide (EDC), N-hydroxysuccinimide (NHS), o-AP, sodium hydroxide (NaOH), phosphate-buffered saline (PBS), sulfuric acid (H_2SO_4), potassium ferrocyanide ($K_3(Fe(CN)_6$), and sodium dodecyl sulfate (SDS), all purchased from Sigma-Aldrich (St. Louis, MO, USA). Selectivity was assessed using standard viral antigens for WSSV (VP28 protein, Creative Diagnostics, USA), norovirus (NoV, VP1 peptide, EastCoast Bio, North Berwick, ME, USA), and rotavirus (RoV, SA-11 antigen, Meridian Bioscience, Newtown, OH, USA), each prepared in PBS solution. Other aqueous reagents were prepared using deionized water (DIW). Field-emission scanning electron microscopy (FE-SEM, Thermofisher, Verios 5 XHR) and Energy Dispersive X-ray Spectroscopy analysis (EDS, Oxford Instruments, AztecLIVE) were used to investigate the sensor surface characterization. Platinum coating (ion sputter coater) was performed at 30 mA for 40 s to obtain high-resolution SEM images.

2.2. Preparation of MIP and NIP sensors

Fig. 1 illustrates the fabrication process of the MIP-based sensor and its quantitative analysis. The gold nano-structured electrode was modified with a chemical cross-linker to immobilize the template molecules. 10 mM 3-MPA was incubated for 90 min, rinsed with DIW, and dried by nitrogen blowing to remove residual materials. Subsequently, 0.2 M EDC/NHS was drop-cast to induce amide bond formation for binding the template molecules. It was followed by incubation for 15 min at room temperature, and before being repeated with a prior washing step **(**Fig. 1**(B), (i))**.

The template molecule was incubated for 1 h, and the unbound residuals were removed using 0.05% PBST (Fig. 1**(B), (ii)**). The 500 ng/mL template molecule was confirmed to provide the optimal cavity **(Fig. S1 (A))**. P(o-AP) was electropolymerized around the electrode surface with the immobilized template molecule **(**Fig. 1**(B), (iii))**.

During electropolymerization, the development of the molecularly imprinted polymer matrix is greatly affected by the cyclic voltammetry (CV) parameters, including the applied potential range, scan rate, and repeated cycle number. These parameters were determined and optimized according to the current change (ΔI) after binding the target molecules with the same concentration **(Fig. S1(B–D))**.

P(o-AP) was synthesized by immersing the electrode in 2 mM o-AP monomer dissolved in 1× PBS (pH = 7.4). CV for electropolymerization was conducted through three repeated scanning cycles at a potential range of – 0.2 to 0.8 V (vs. Ag/AgCl) and a scan rate of 50 mV/s. During electropolymerization, the peak current gradually decreased with increasing cycles owing to the formation of a relatively weakly conductive film **(Fig. S2)**. The template molecule was later removed from the electropolymerized o-AP film using a suitable eluent, generating vacant molecular cavities (Fig. 1**(B), (iv)**).

Fig. S3 shows the optimized eluent and rebinding conditions. First, the electrode surfaces were treated with acidic (H_2SO_4) or alkaline (NaOH) elution of 5 mM for a certain time before being washed with PBS and dried with nitrogen gas. The NaOH presented noticeable current changes (ΔI) along the left axis in **Fig. S3(A)**. The NIP sensor presented no current changes in acidic or alkaline solutions, reflecting the lack of damage to the thin P(o-AP) film. After incubating the target molecule, the MIP sensor assessed the recognition ability using the imprinting factor (IF), which followed the right axis compared to the NIP sensor. Despite the same concentration, a remarkable difference was observed between the NaOH (16.2) and H_2SO_4 (6.4) eluents. The reagents and cyclic voltammetry (CV) parameters applied in this study were referenced from previous studies on electropolymerization-based MIP sensors using o-aminophenol, which follow a similar approach [17,38,39]. Also, 0.05 % SDS was added with NaOH to efficiently remove the template molecule and prevent non-specific adsorption [32,33]. We assessed the current change (ΔI) associated with different target

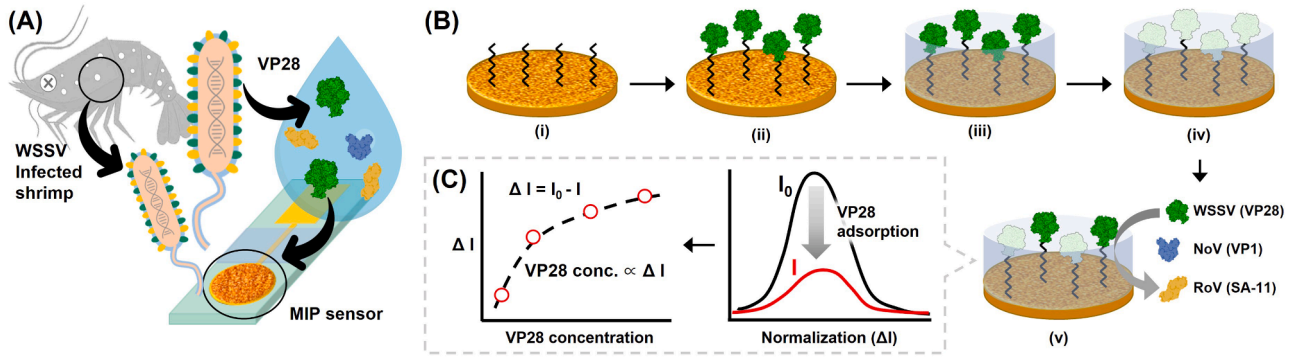

Fig. 1. Preparation of P(o-AP)-based VP28 detection sensor and its experimental analysis. (A) Target material and detection platform. (B) Sensor fabrication: (i) chemical functionalization on the gold nanostructured electrode, (ii) template immobilization, (iii) electropolymerization using o-aminophenol (o-AP), (iv) template elution, (v) rebinding with the target molecule, and (C) electrochemical signal analysis and quantification.

molecules (WSSV [VP28]-red column) compared to the interfering molecules (NoV [VP1]-black column) in the MIP sensor **(Fig. S3(B))**. After incubating for 8 min, we confirmed that the 5 mM NaOH and 0.05 % SDS eluent caused the most significant current change, 5.17 μA, whereas the interfering molecule had an IF of 1.55 μA.

Next, the elution and rebind times were verified based on the current change over time **(Fig. S3(C), (D))**. During the elution process in the MIP sensor, the current change gradually increased between 2 and 8 min, confirming 8 min as the optimal elution time. On the other hand, the NIP sensor displayed a negligible current change, which means that the P(o-AP) film was rarely damaged during the elution procedure. The rebinding target molecules have indicated the maximum current change of 8.33 μA at 15 min.

The non-imprinted polymer (NIP) sensor did not include the template molecule in the polymer film. Thus, it was fabricated following the same process except for the template removal step. The electrochemical responses of the prepared MIP and NIP sensors were determined through differential pulse voltammetry (DPV) sensing of redox ions (Fig. 1**(B), (v)**). Also, we analyzed the current changes (ΔI) associated with the different concentrations of the target molecule (Fig. 1**(C)**).

2.3. Real sample analysis

We investigated the applicability of the MIP sensor for quantitatively detecting VP28 in real samples. The virus concentration (copies/mL) was verified in all samples using a standard qPCR kit (IQ REAL WSSV, GeneReach Biotechnology). WSSV-infected shrimp and aquaculture water were obtained from an aquaculture farm in Yeosu, South Korea.

First, shrimp samples were homogenized by centrifugation at 3,000 rpm for 3 min using 10 g of pleopods in 10 mL of 0.1% Triton X-100. The homogenized samples were centrifuged at 10,000 rpm for 30 min, and the supernatant was gathered. The aquaculture water samples were centrifuged at 10,000 rpm for 30 min, and the homogenization step was skipped. All samples were highly saline, which reduces the affinity of the imprinted cavities and provokes non-specific binding [40,41]. Therefore, aquaculture water with an extremely low virus concentration was utilized as a control sample to study the effect of salinity. Aquaculture water samples with different dilution ratios were used to measure the response signal against 50 ng/mL VP28 **(Fig. S4)**. Because the 100-fold dilution ratio displayed a prominent response signal for VP28, the same dilution ratio was applied in later experiments.

3. Results and discussion

3.1. Electrochemical characterization

We assessed the electrochemical behaviors using CV and electrochemical impedance spectroscopy (EIS) after electrode modification and target molecule adsorption.

The DPV curves showed a typical oxidation peak during sensor fabrication (measured in PBS solution containing 5 mM $[Fe(CN)_6]^{3-/4-}$ (Fig. 2**(A)**). After immobilizing the template molecule, the oxidation peak current decreased to a potential of ~0.24 V, indicating that it interfered with electron transfer. Next, the P(o-AP) synthesis generates an almost flat curve due to the low conductivity of the surface-coated electropolymerization. The synthesized P(o-AP) formed and interacted around the template molecule, developing a particular three-dimensional structure. The template molecule was then effectively extracted from the P(o-AP) film.

The oxidation peak current in the MIP sensor decreased again after rebinding the target molecule (50 ng/mL), indicating that the imprinted cavities on the film surface establish non-covalent bonds with the adsorbed target molecules, thereby blocking the movement of redox ions on the sensor surface. In contrast, the NIP sensor did not display a peak current after rebinding the target molecule because it did not provide the imprinted cavities (Fig. 2**(B)**).

EIS was conducted to verify the non-specific adsorption (Fig. 2**(C), (D)**). The Nyquist plot was measured with a 5-mV amplitude, a potential of + 0.259 V, and a frequency range from 0.1 to 100 kHz in an electrolyte of 0.1 M PBS. The semicircular curve in the high-frequency region indicated successful electron transfer at the sensor surface. The linear curve in the low-frequency region represents the diffusion between the interfacial solution and the sensor surface. The plot was fitted with the constant phase element (CPE) with diffusion circuit model, which considers the solution resistance (R_s), and Warburg impedance (W).

The Nyquist plot for each fabrication step of the MIP sensor revealed that electron transfer resistance (Rct) continuously increased from modifying the gold nanostructured electrode to synthesizing P(o-AP) films. The template elution decreased the Rct to 1462 Ω, indicating effective electron transfer at the imprinted sites. After incubation of the MIP sensor with the target molecules for 15 min, the Rct increased to 1537 Ω, suggesting that the imprinted sites enable specific recognition (Fig. 2**(C)**). In contrast, the NIP sensor showed little change in Rct before and after target molecule adsorption (1506 Ω and 1507 Ω, respectively), indicating its lack of selective recognition and binding abilities (Fig. 2 **(D)**). These findings suggested that the MIP sensor can specifically recognize and rebind target molecules.

3.2. Surface characterization

FE-SEM and EDS analyses were performed to characterize the surface morphology and elemental composition of (i) the GNE, (ii) the P(o-AP), and (iii) the MIP-modified electrode, as shown in Fig. 3. In the SEM images (A), the electropolymerized P(o-AP) and MIP exhibited relatively thicker and blunter surface structures compared to the unmodified GNE.

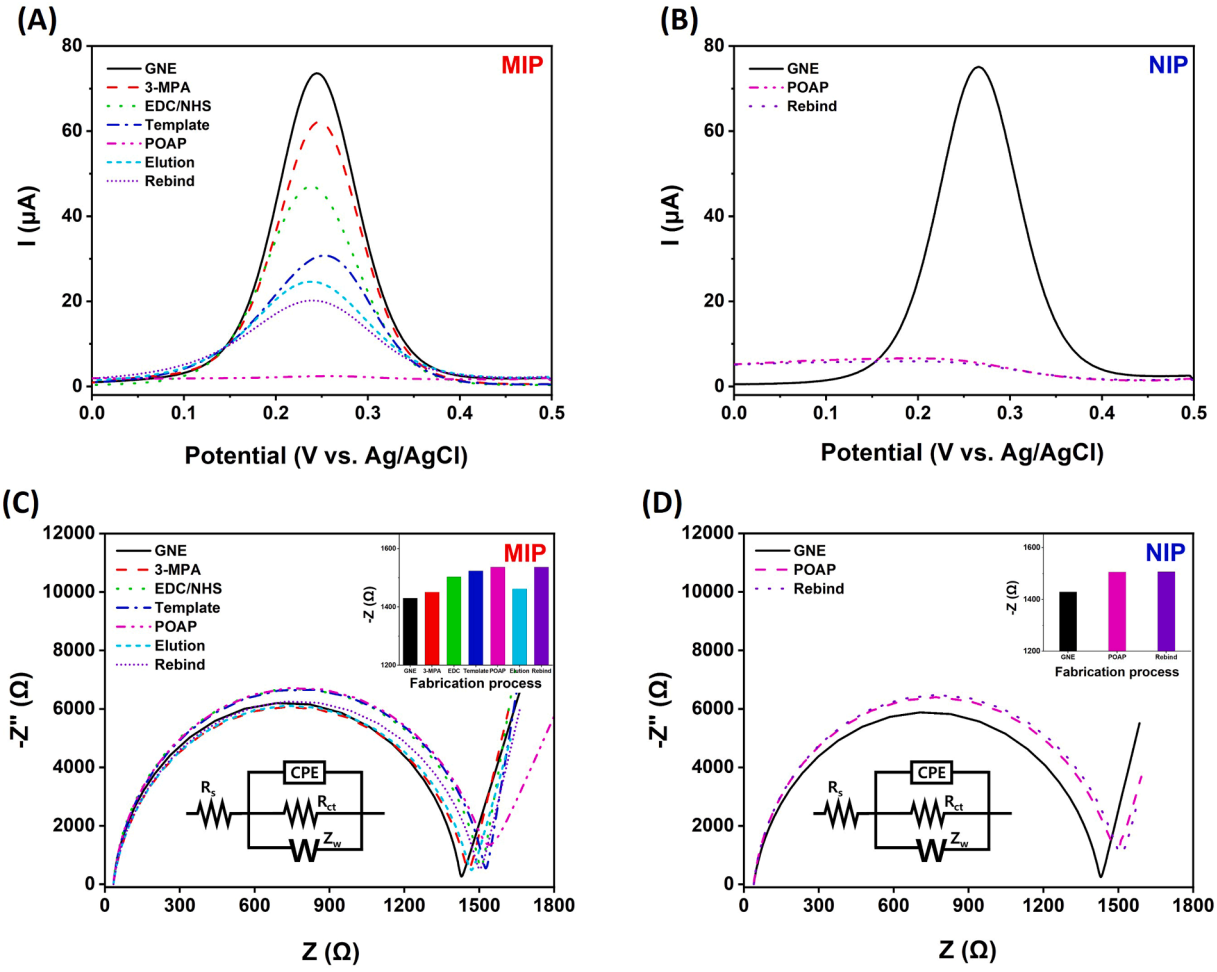

Fig. 2. Electrochemical responses of sensors with and without electrode modification. (A, B) Differential pulse voltammograms (DPVs) were recorded in a 5-mM $[Fe(CN)_6]^{3-/4-}$ solution. (C, D) Nyquist electrochemical impedance spectroscopy (EIS) diagrams were recorded in 0.1 M phosphate buffer solution (pH 7.4).

This suggests that the polymer deposition was successful on the electrode surface. Elemental mapping images (B) revealed a homogeneous distribution of C, N, and O on the P(o-AP) and MIP surfaces; however, the Au signals were more dominant and exposed in the GNE. This indicates the GNE was effectively covered by the polymer film after electropolymerization. In the EDS spectrum (C), both P(o-AP) and MIP electrodes showed increased C, N, and O signals, while Au peak intensity decreased compared with the GNE. It confirms the deposition of the polymer film on the surface. Notably, the weight percentages (Wt%) of the C, N, and O in the MIP were similar to those of the P(o-AP). It displayed only a slight C and N decrease and a minor O peak increase. This is likely attributed to increased surface exposure to the atmosphere after elution. The consistent elemental composition and morphology between the P(o-AP) and MIP suggest that the polymer film remained structurally stable and was not significantly damaged during elution.

3.3. Analytical response

The MIP sensor was quantitatively analyzed using DPV in the presence of a redox probe solution. VP28 (incubated with the sensor at 0.78–50 ng/mL) occupied the imprinted cavities of the MIP sensor during the rebinding process. It hindered the electron transfer of the probe ions and generated a decreasing peak current. The peak current obtained from DPV was calculated as $\Delta I = I_0 - I$ to normalize the response signal (ΔI), which we fitted using the Langmuir–Freundlich adsorption model for the various VP28 concentrations. More imprinted cavities were occupied with increasing VP28 concentration, causing a proportional decrease in peak current within the same rebinding time (Fig. 4**(A)**). The calibration curve of the MIP sensor exhibited a high correlation coefficient of $R^2 = 0.95$ (Fig. 4**(B)**). As expected, the NIP sensor did not show a noticeable response signal because it does not have the imprinted cavities for VP28 binding.

The LoD was calculated as follows: $\text{LoD} = (3 \times \sigma) / S$, where σ is the standard deviation of the y-intercept of the regression line, and S is the slope of the calibration curve [42]. It has found a LoD of 7.01 ng/mL. We calculated the IF to estimate the binding affinity and selectivity of the imprinting cavities within the polymer film. IF > 1 indicates that the imprinted cavities are appropriately designed and have reliable selectivity, whereas IF ≈ 1 or < 1 demonstrates that the imprinting cavities are non-specific and have inapposite selectivity [43,44]. Accordingly, the capability of the MIP sensor for recognizing VP28 was calculated as follows: IF $= \Delta I_{sat}$ MIP / ΔI_{sat} NIP, where ΔI_{sat} indicates the saturated current response. At an IF of 4.35, the P(o-AP) film of the MIP sensor demonstrated effective imprinting of VP28. Also, the reusability was conducted following repeated detection and elution cycles using a single electrode. The signal intensity variation over three consecutive cycles was maintained within 13%. These results support the potential reusability of the electrode **(Fig. S5)**. These results indicated that the MIP sensor can specifically recognize and bind the target molecule VP28 with high sensitivity, reflecting its excellent potential in diagnostic applications.

Many studies have reported the WSSV antigen-based detection method and have compared it with the detection range, LoD, and assay time shown in Table 1. Compared to previous technologies, the MIP

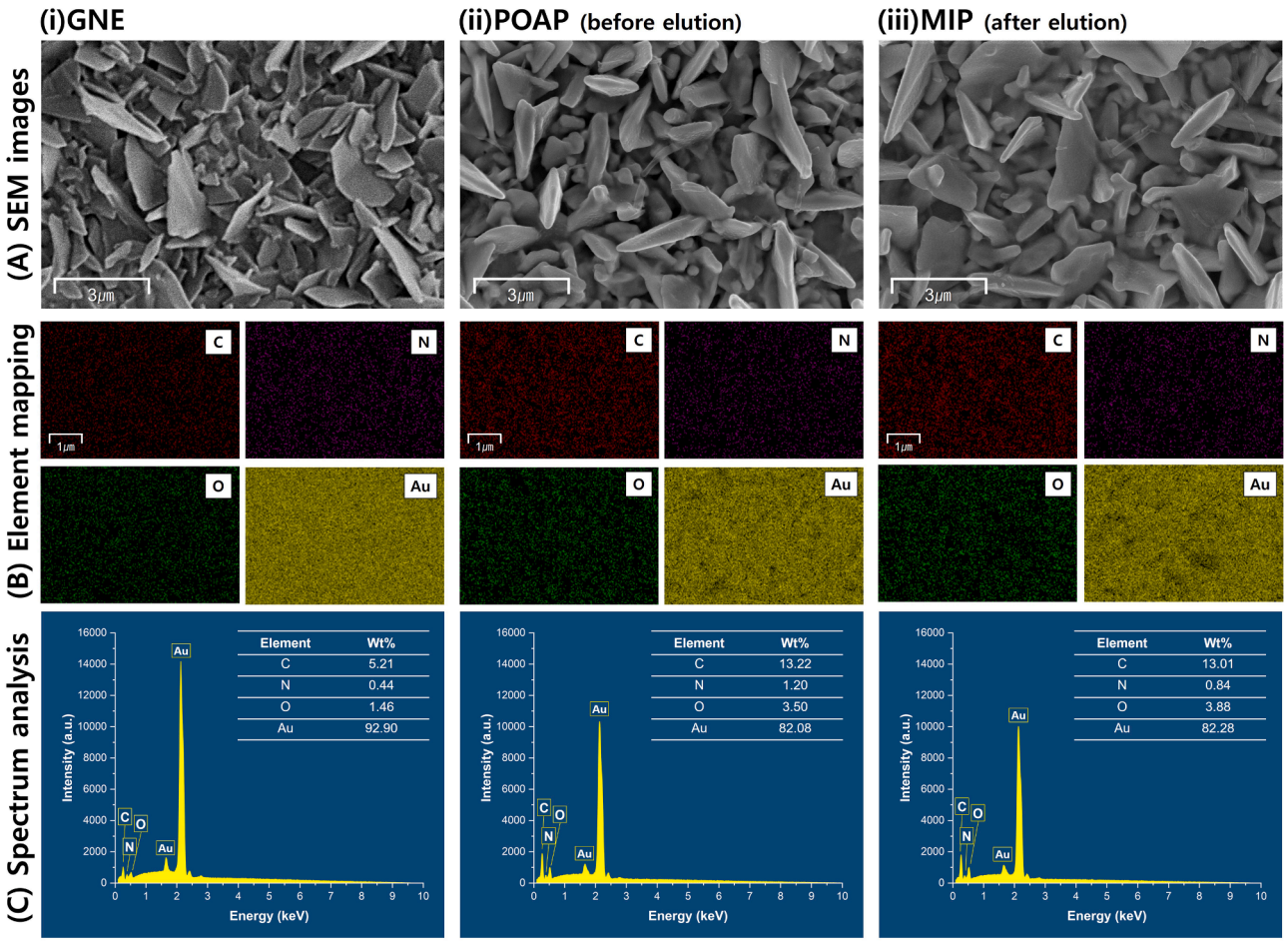

Fig. 3. (A) SEM images, (B) Elemental mapping images, and (C) Spectrum analysis of (i) GNE, (ii) P(o-AP), and (iii) MIP modified electrodes.

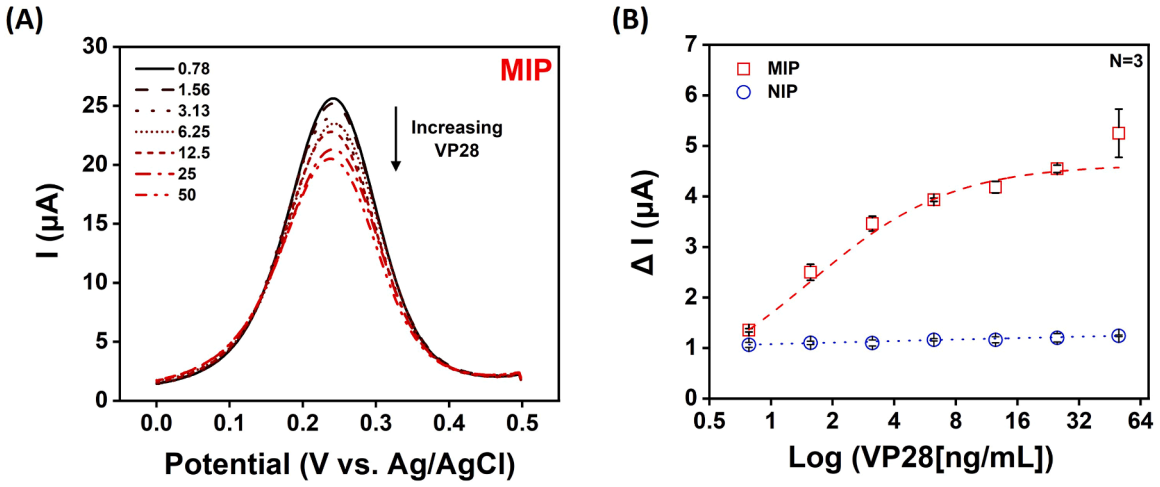

Fig. 4. MIP sensing properties. (A) DPVs and (B) their calibration plots for the MIP and NIP electrodes in 1× PBS spiked with VP28 (0.78–50 ng/mL). Electrochemical measurements were performed in a 5-mM $[Fe(CN)_6]^{3-/4-}$ solution.

sensor provides an antibody-less, cost-effective, short assay time, and an easy-to-fabricate solution. It can be adapted as an efficient and reasonable sensing platform for quantitatively detecting viral biomarkers.

3.4. Selectivity study

We examined the selectivity of the MIP sensor using target [WSSV (VP28, 25 kDa)] and interference antigens [NoV (VP1, 58 kDa), RoV (SA-11, 38 kDa)]. These antigens are attributed to viral infection in shrimp and aquaculture environments [48]. All antigens were prepared in 1× PBS solution at the same concentration range and measured under the same experimental conditions (Fig. 5). The selectivity of the sensor was estimated as the ratio of response signals for the target (VP28) and interference antigens (VP1, SA-11): Selectivity coefficient ($K_{target,}$

Table 1
Comparison of WSSV antigen-based detection methods.

Method	Detection range	LoD	Assay time	Refs.
LFIA[a]	0.042–224 μg/mL	12.5 μg/mL	20 min	[2]
LFIA	0.8–4 ng/mL	4 ng/mL	15 min	[45]
Immuno-dot blot	0.25–200 ng/mL	1 ng/mL	4 h	[46]
Impedimetric sensor	10–1000 ng/mL	25 ng/mL	30 min	[47]
	0-60 ng/mL	2.4 ng/mL	1 h	[41]
MIP-based sensor	0.78–50 ng/mL	7 ng/mL	15 min	This study

[a] LFIA, lateral flow immunoassay

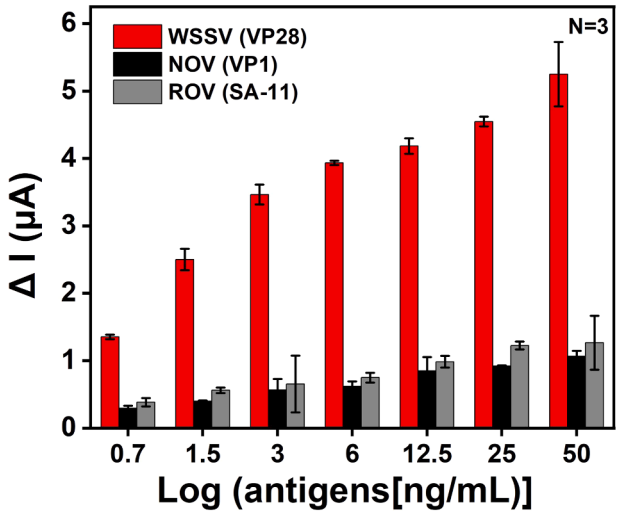

Fig. 5. Selectivity study for WSSV, NoV, and RoV antigens (0.78–50 ng/mL in PBS). The plots show the normalized peak currents (Δ*I*) from DPV in 5 mM $[Fe(CN)6]^{3-/4-}$ solution.

$_{interference}) = \Delta I_{conc.}$ WSSV / $\Delta I_{conc.}$ NoV, RoV, where ΔI_{conc} indicates the current changes for the target or interference antigens at particular concentrations. The selectivity for VP28 compared to VP1 ($K_{WSSV,\ NoV}$) was an average of 5.4. The selectivity for VP28 compared to SA-11 ($K_{WSSV,\ RoV}$) was an average of 4.4. The selectivity coefficients at 0.7–50 ng/mL of the target and interference antigens are presented in Fig. 5 and **Table S1**. The results indicated that the imprinted cavities of the MIP sensor provide a strong affinity for complementary binding interactions with the target antigen. Our sensor showed remarkable selectivity and verifiable detection performance among the interference antigens and thus represents a promising platform for sensitive and selective detection of VP28.

3.5. Real sample analysis

We compared the performance of the MIP sensor for real sample analysis to the standard qPCR method. The sensor responses were evaluated according to the peak current using DPV and presented as the normalized Δ*I*. qPCR indicated that the pleopod-containing samples (#1 and #2) had a virus concentration of 925.8 and 252.5 × 10^6 copies/mL, respectively (Fig. 6). The sensor showed a proportionally similar difference between these samples (6.5 and 2.5 μA, respectively). qPCR did not detect any virus particles in the water samples (#3 and #4). In contrast, the sensor exhibited electrochemical current signals of 0.35 and 0.37 μA, which were assumed to reflect non-specific binding or noise signals. These results suggested that the MIP sensor has a highly similar detection performance to standard qPCR for infected shrimp and aquaculture water.

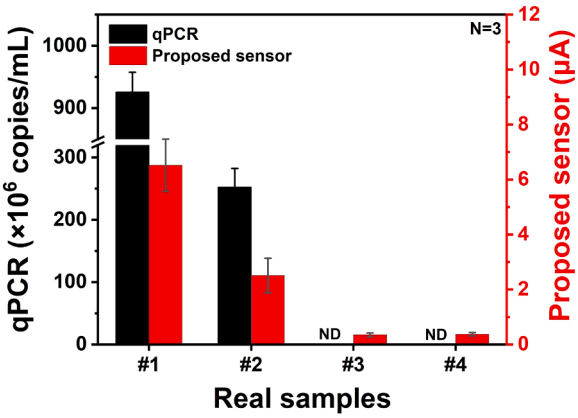

Fig. 6. Comparison of MIP sensor and qPCR for WSSV detection in real samples. The qPCR results are shown on the left y-axis (black columns), while the proposed sensor responses are displayed on the right y-axis (red columns). Samples #1 and #2 represent WSSV-infected pleopods, while samples #3 and #4 represent aquaculture water. ND, not detected.

4. Conclusions

In this study, we developed an MIP-based electrochemical sensor to quantitatively detect VP28 as a WSSV biomarker. Our sensor was designed based on an existing molecular recognition technology and P(o-AP) electropolymerized on a gold nanostructured electrode with a large surface area for high electron transfer rates.

The MIP sensor showed stronger response signals than the NIP sensor, and its detection performance proportionally changed following the target antigen VP28 concentration. The sensor had a detection limit of 7.0 ng/mL, showing excellent sensitivity compared to the other platforms. Moreover, the sensor selectively recognized the WSSV antigen among interference antigens.

These findings indicate that the optimized sensor detected VP28 with high accuracy, sensitivity, selectivity, and simplicity. The platform shows stable performance despite interference in complex biological samples. Therefore, the MIP-based electrochemical biosensor represents a practicable and reliable approach for the early and real-time detection of various viral biomarkers, including WSSV. This advancement can promote prompt monitoring and effective virus management in the aquaculture industry.

Funding sources

This work was supported by the National Research Foundation of Korea (NRF) grant funded by the Korea government (MSIT) (No. NRF-2021R1A2C3008169).

CRediT authorship contribution statement

Young-Ran Yun: Writing – original draft, Validation, Methodology, Investigation, Formal analysis, Data curation, Conceptualization. **Hyoung Jun Kim:** Resources. **Sung Yang:** Writing – review & editing, Supervision, Conceptualization.

Declaration of competing interest

The authors declare that they have no known competing financial interests or personal relationships that could have appeared to influence the work reported in this paper.

Supplementary materials

Supplementary material associated with this article can be found, in

the online version, at doi:10.1016/j.snr.2025.100375.

Data availability

The data that has been used is confidential.

References

[1] M.C. van Hulten, et al., White spot syndrome virus envelope protein VP28 is involved in the systemic infection of shrimp, Virology 285 (2) (2001) 228–233.
[2] P.K. Kulabhusan, et al., Lateral flow assay for rapid detection of white spot syndrome virus (WSSV) using a phage-displayed peptide as bio-recognition probe, Appl. Microbiol. Biotechnol. 101 (2017) 4459–4469.
[3] K. Takemura, et al., Electrochemical detection of white spot syndrome virus with a silicone rubber disposable electrode composed of graphene quantum dots and gold nanoparticle-embedded polyaniline nanowires, J. Nanobiotechnol. 18 (2020) 1–12.
[4] H. Gong, et al., Portable paper-based molecularly imprinted sensor for visual real-time detection of influenza virus H5N1, Chem. Eng. J. 477 (2023) 146990.
[5] H. Gong, et al., Ultra-sensitive portable visual paper-based viral molecularly imprinted sensor without autofluorescence interference, Anal. Chem. 95 (48) (2023) 17691–17698.
[6] G. Cai, et al., A point-to-point “cap” strategy to construct a highly selective dual-function molecularly-imprinted sensor for the simultaneous detection of HAV and HBV, Biosens. Bioelectron. 219 (2023) 114794.
[7] W.-T. Ting, M.-J. Wang, M.M. Howlader, Interleukin-6 electrochemical sensor using poly (o-phenylenediamine)-based molecularly imprinted polymer, Sens. Actuat. B 404 (2024) 135282.
[8] V. Ayerdurai, M. Cieplak, W. Kutner, Molecularly imprinted polymer-based electrochemical sensors for food contaminants determination, TrAC Trends Anal. Chem. 158 (2023) 116830.
[9] D. Campagnol, et al., Molecularly imprinted electrochemical sensor for the ultrasensitive detection of cytochrome c, Bioelectrochemistry 148 (2022) 108269.
[10] Y. Li, et al., Recent advances in molecularly imprinted polymer-based electrochemical sensors, Biosens. Bioelectron. 249 (2024) 116018.
[11] M. Agar, et al., Aptamer-molecularly imprinted polymer sensors for the detection of bacteria in water, Biosens. Bioelectron. 272 (2025) 117136.
[12] J.G. Pacheco, et al., Breast cancer biomarker (HER2-ECD) detection using a molecularly imprinted electrochemical sensor, Sens. Actuat. B 273 (2018) 1008–1014.
[13] R.D. Crapnell, et al., Molecularly imprinted polymer based electrochemical biosensors: overcoming the challenges of detecting vital biomarkers and speeding up diagnosis, Talanta Open. 2 (2020) 100018.
[14] S. Ansari, S. Masoum, Molecularly imprinted polymers for capturing and sensing proteins: current progress and future implications, TrAC Trends Anal. Chem. 114 (2019) 29–47.
[15] R. Ciriello, et al., Improved stability of thin insulating poly (o-aminophenol) films in aqueous solutions through an efficient strategy for electrosynthesis under neutral pH conditions: electrochemical and XPS investigation, J. Electroanal. Chem. 867 (2020) 114183.
[16] R. Elshafey, G.F. Abo–Sobehy, A.E. Radi, A sensitive molecularly imprinted poly (o-aminophenol)-based electrochemical sensor for propiconazole in food samples using reduced graphene oxide-chitosan composite, Microchem..J. 212 (2025) 113255.
[17] H. Chasta, R.N. Goyal, Molecularly imprinted sensor based on o-aminophenol for the selective determination of norepinephrine in pharmaceutical and biological samples, Talanta 125 (2014) 167–173.
[18] S. Menon, S. Jesny, K.G. Kumar, A voltammetric sensor for acetaminophen based on electropolymerized-molecularly imprinted poly (o-aminophenol) modified gold electrode, Talanta 179 (2018) 668–675.
[19] L.-J. Kong, et al., An electrochemical sensor for rapid determination of ractopamine based on a molecularly imprinted electrosynthesized o-aminothiophenol film, Anal. Bioanal. Chem. 404 (2012) 1653–1660.
[20] P.V. Shine, et al., Epitope mapping of the White Spot Syndrome Virus (WSSV) VP28 monoclonal antibody through combined in silico and in vitro analysis reveals the potential antibody binding site, Mol. Cell Probes. 50 (2020) 101508.
[21] C.-l. Hou, et al., Characterization and diagnostic use of a monoclonal antibody for VP28 envelope protein of white spot syndrome virus, Virol. Sin. 26 (2011) 260–266.
[22] X. Tang, et al., Crystal structures of major envelope proteins VP26 and VP28 from white spot syndrome virus shed light on their evolutionary relationship, J. Virol. 81 (12) (2007) 6709–6717.
[23] A.G. Ayankojo, et al., Molecularly imprinted polymer based electrochemical sensor for quantitative detection of SARS-CoV-2 spike protein, Sens. Actuat. B 353 (2022) 131160.
[24] M. Antipchik, et al., MIP-based electrochemical sensor for direct detection of hepatitis C virus via E2 envelope protein, Talanta 250 (2022) 123737.
[25] A. Raziq, et al., Development of a portable MIP-based electrochemical sensor for detection of SARS-CoV-2 antigen, Biosens. Bioelectron. 178 (2021) 113029.
[26] M.S. Silva, et al., Rational selection of hidden epitopes for a molecularly imprinted electrochemical sensor in the recognition of heat-denatured dengue NS1 protein, Biosens. Bioelectron. 191 (2021) 113419.
[27] M.S. Sengar, et al., Molecularly imprinted polymer technology for the advancement of its health surveillances and environmental monitoring, ACS Appl. Polym. Mater. 6 (2) (2024) 1086–1105.
[28] M.S. Sengar, et al., Molecularly imprinted polymer technology for the advancement of its health surveillances and environmental monitoring, ACS Appl. Polym. Mater. (2024).
[29] L. Liu, et al., Improvement of the homogeneity of protein-imprinted polymer films by orientated immobilization of the template, Anal. Chim. Acta 726 (2012) 85–92.
[30] Y. Fang, et al., Simultaneous electrochemical determination of nitrophenol isomers Based on spirofluorene-based microporous polymer film modified electrodes through one-step electropolymerization strategy, Sens. Actuat. B 333 (2021) 129568.
[31] S.M. Cerqueira, et al., Development of an electrochemical biosensor for Galectin-3 detection in point-of-care, Microchem. J. 164 (2021) 105992.
[32] A. Herrera-Chacón, X. Cetó, M. Del Valle, Molecularly imprinted polymers-towards electrochemical sensors and electronic tongues, Anal. Bioanal. Chem. 413 (2021) 6117–6140.
[33] M.A. Tabrizi, et al., An ultrasensitive molecularly imprinted polymer-based electrochemical sensor for the determination of SARS-CoV-2-RBD by using macroporous gold screen-printed electrode, Biosens. Bioelectron. 196 (2022) 113729.
[34] S. Motia, et al., Synthesis and characterization of a highly sensitive and selective electrochemical sensor based on molecularly imprinted polymer with gold nanoparticles modified screen-printed electrode for glycerol determination in wastewater, Talanta 216 (2020) 120953.
[35] E. Han, et al., Flower-like molecularly imprinted nanocomposite based on ZnO@Au for sensitive and selective electrochemical sensing of tert-butylhydroquinone, Talanta (2025) 127989.
[36] X. Zhang, et al., A novel electrochemical sensor based on electropolymerized molecularly imprinted polymer and gold nanomaterials amplification for estradiol detection, Sens. Actuat. B 200 (2014) 69–75.
[37] Y.-R. Yun, et al., Sensitive electrochemical immunosensor to detect prohibitin 2, a potential blood cancer biomarker, Talanta 238 (2022) 123053.
[38] J. Li, J. Zhao, X. Wei, A sensitive and selective sensor for dopamine determination based on a molecularly imprinted electropolymer of o-aminophenol, Sens. Actuat. B 140 (2) (2009) 663–669.
[39] R. Ciriello, et al., Electrosynthesized poly (o-aminophenol) films as biomimetic coatings for dopamine detection on Pt substrates, Chemosensors 9 (10) (2021) 280.
[40] T. Matsunaga, T. Hishiya, T. Takeuchi, Surface plasmon resonance sensor for lysozyme based on molecularly imprinted thin films, Anal. Chim. Acta 591 (1) (2007) 63–67.
[41] H. Kempe, M. Kempe, Influence of salt ions on binding to molecularly imprinted polymers, Anal. Bioanal. Chem. 396 (2010) 1599–1606.
[42] A. Shrivastava, V.B. Gupta, Methods for the determination of limit of detection and limit of quantitation of the analytical methods, Chron. Young Sci. 2 (1) (2011) 21–25.
[43] X. Hu, et al., An effective ratiometric electrochemical sensor for highly selective and reproducible detection of ochratoxin A: Use of magnetic field improved molecularly imprinted polymer, Sens. Actuat. B 359 (2022) 131582.
[44] M. Frigoli, et al., Thermal pyocyanin sensor based on molecularly imprinted polymers for the indirect detection of Pseudomonas aeruginosa, ACS Sens. 8 (1) (2023) 353–362.
[45] J.C.-K. Hsu, et al., Diagnostic performance of a Rapid Test Kit for white spot syndrome virus (WSSV), Aquaculture 558 (2022) 738379.
[46] C. Thiruppathiraja, et al., An enhanced immuno-dot blot assay for the detection of white spot syndrome virus in shrimp using antibody conjugated gold nanoparticles probe, Aquaculture 318 (3-4) (2011) 262–267.
[47] S. Sannigrahi, et al., Detection of white spot syndrome virus in seafood samples using a magnetosome-based impedimetric biosensor, Arch. Virol. 166 (2021) 2763–2778.
[48] G. Javdani Shahedin, et al., Prevalence of enteric viruses in raw seafood collected from the retail shops in Tehran, Iran, 2022–2023, Iran. J. Med. Microbiol 18 (3) (2024) 190–199.